minerals

MDPI

Article

Tracing Pre-Mesozoic Tectonic Sutures in the Crystalline Basement of the Protocarpathians: Evidence from the Exotic Blocks from Subsilesian Nappe, Outer Western Carpathians, Poland

Jan Golonka [1,*], Aleksandra Gawęda [2], Anna Waśkowska [1], David Chew [3], Krzysztof Szopa [2] and Foteini Drakou [3]

[1] Geophysics and Environmental Protection, Faculty of Geology, AGH University of Science and Technology, al. A. Mickiewicza 30, 30-059 Krakow, Poland; waskowsk@agh.edu.pl
[2] Institute of Earth Sciences, University of Silesia in Katowice, Będzińska 60, 41-200 Sosnowiec, Poland; aleksandra.gaweda@us.edu.pl (A.G.); krzysztof.szopa@us.edu.pl (K.S.)
[3] Department of Geology, School of Natural Sciences, Trinity College Dublin, Dublin 2, Ireland; chewd@tcd.ie (D.C.); drakouf@tcd.ie (F.D.)
* Correspondence: jgolonka@agh.edu.pl; Tel.: +48-50-501-72-83

Abstract: Pre-Mesozoic exotic crystalline blocks within the Outer Carpathian flysch have potential to unravel the nature of their eroded basement source(s) and to reconstruct the Paleozoic–Precambrian history of the Protocarpathians. Strongly tectonized Campanian–Maastrichtian grey marls in the Subsilesian Nappe of the Outer Western Carpathians in Poland contain a variety of different lithology types, including granitoids and andesites. Petrological investigations coupled with zircon and apatite U-Pb dating were performed on crystalline (subvolcanic) exotic blocks from a locality in the Subsilesian Nappe. U-Pb zircon dating yields magmatic crystallization ages of c. 293 Ma for the microgranitoid and c. 310 Ma for the andesite block, with inherited zircon cores yielding Archean, Paleoproterozoic, Mesoproterozoic and Cadomian ages. Whole rock trace element and Nd isotope data imply that the melt source was composed of a significant Neoproterozoic crustal component in both the microgranite and andesite. The Late Carboniferous–Permian magmatic activity likely continues outside the Carpathian Belt and can be linked to a Late Paleozoic transtensional zone, which is a continuation of the Lubliniec–Kraków Zone that extends under the Carpathians to Moesia. This Late Paleozoic transtensional zone was probably reactivated during the Late Cretaceous under a transpressional regime within the Żegocina tectonic zone, which caused the uplift of the Subsilesian Ridge and intensive erosion.

Keywords: exotic blocks; U-Pb zircon dating; Subsilesian Nappe; Outer Western Carpathians

check for updates

Citation: Golonka, J.; Gawęda, A.; Waśkowska, A.; Chew, D.; Szopa, K.; Drakou, F. Tracing Pre-Mesozoic Tectonic Sutures in the Crystalline Basement of the Protocarpathians: Evidence from the Exotic Blocks from Subsilesian Nappe, Outer Western Carpathians, Poland. *Minerals* **2021**, *11*, 571. https://doi.org/10.3390/min11060571

Academic Editor: Alexey V. Ivanov

Received: 16 April 2021
Accepted: 25 May 2021
Published: 27 May 2021

1. Introduction

The presence of Pre-Mesozoic basement within the Alpine orogens was first identified c. 200 years ago [1]. In most of the Alpine orogens of Europe, such as the Alps and Carpathians, Pre-Mesozoic basement is present as exotic blocks inside the sedimentary or metasedimentary successions or as uplifted crystalline massifs, termed "core mountains" [2,3]. Investigating the Pre-Alpine basement and constraining the timing of its main tectonic events remain active problems in European geology. The Carpathian Mountains are an orogen of Alpine (Cretaceous–Neogene) age, but their structure reflects a prolonged Neoproterozoic and Phanerozoic history. While the crystalline massifs in the Central Carpathians are relatively well-studied ([3] and references therein), the presence of pre-Alpine components in the Outer Carpathians are less understood. Pre-Alpine basement is present in the form of exotic blocks and interpreted as remnants of the Protocarpathian crystalline basement, which is inferred to underlay the Mesozoic and Cenozoic basins of the Carpathian orogenic

system [4,5]. During the syn-orogenic (Cretaceous–Neogene) stage of the evolution of the Carpathians, several ridges were formed inside the Tethys marginal basins [6]. These ridges were cored by Pre-Mesozoic crystalline basement and were uplifted during Alpine closure of the Tethys Ocean. Subsequent erosion of the uplifted ridges resulted in the transportation of large amounts of basement material (often as olistostromes) into the Carpathian basins [7]. These crystalline blocks likely represent remnants of the Protocarpathian basement and afford the opportunity to reconstruct the Neoproterozoic to Paleozoic–Precambrian history of the Protocarpathians. This paper investigates and interprets crystalline plutonic and volcanic exotic blocks, found at a locality in the Subsilesian Nappe of the Outer Western Carpathians in Poland (Figure 1).

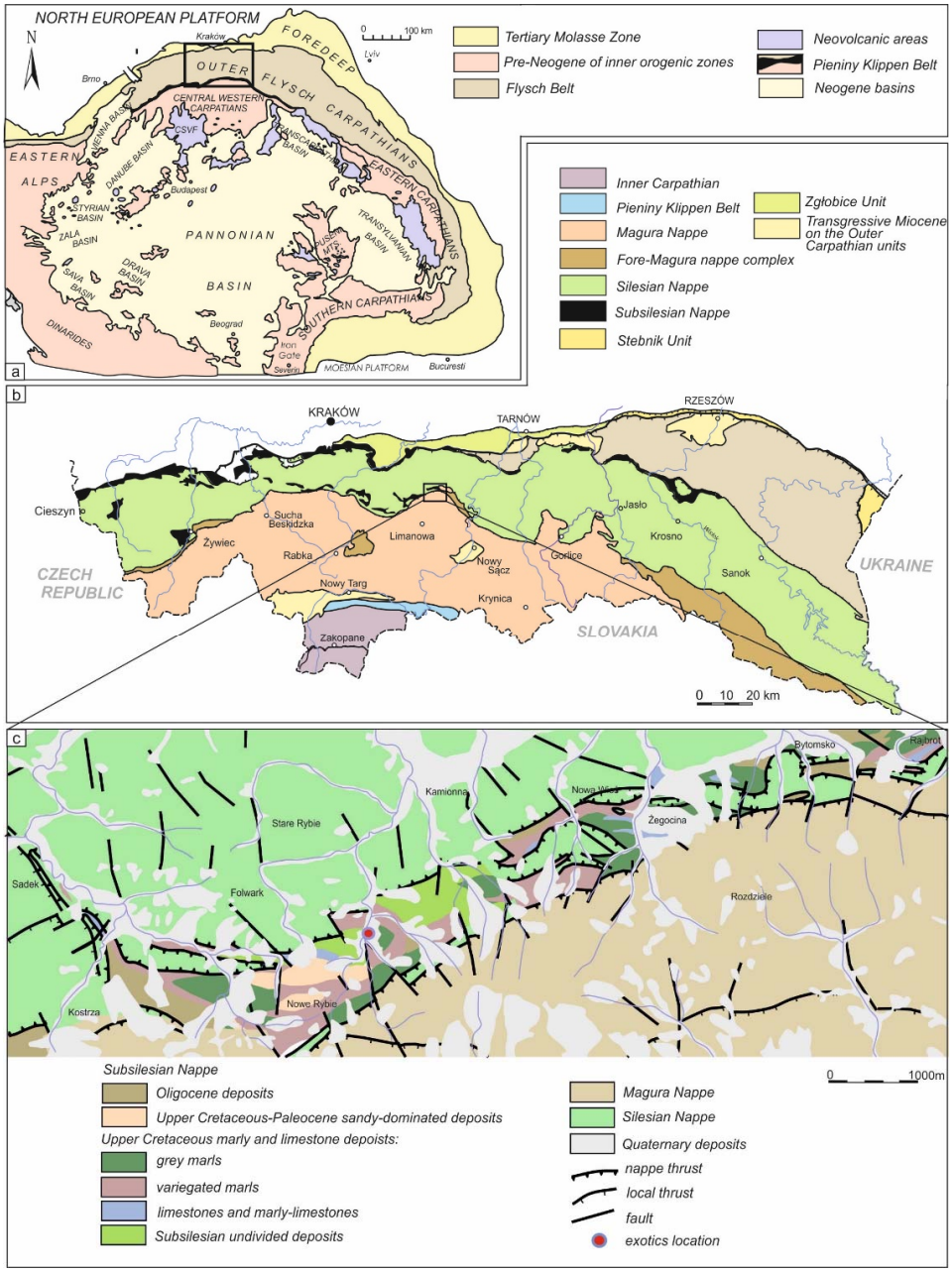

Figure 1. Location of the study area on (**a**) a simplified geological map of the Carpathian chain within Europe, (**b**) the general geological structure of Carpathians in Poland (map constructed using information included in [3–5,8] and (**c**) on a detailed geological map of the Żegocina Zone (constructed using information included in [9]).

2. Geological Setting and Sampling

The Carpathian Mountains in the Czech Republic, Poland, Slovakia, Ukraine and Romania are geographically divided into the Western, Eastern and Southern Carpathians (Figure 1a). The Western Carpathians in Poland are traditionally subdivided into the Central and Outer Carpathians, separated by the Pieniny Klippen Belt ([3] and references therein; [10]). The Outer Western Carpathians are built of Jurassic–Neogene sedimentary rocks that were thrust over the European Platform (Figure 1a,b). This resulted in the formation of nappe sequences that detached from their basement [11,12] and comprise the Magura Nappe, Fore–Magura Group of nappes, Silesian Nappe, Subsilesian Nappe and Skole (Skiba) Nappe (Figure 1b). These sedimentary sequences often contain crystalline exotic blocks. In the Subsilesian and Silesian nappes, most of the exotic blocks are of Neoproterozoic age [5,13,14], while the basement of Magura Nappe, as deduced from exotic blocks, is primarily late Variscan with Neoproterozoic remnants [15]. The analysed exotic blocks are shown in Figure 2.

Figure 2. Photographs of the exotic blocks from Pluskawka Stream, with their microstructures: (**a**) Pl 2 microgranitoid block, in situ within the marl (exposure in Pluskawka Stream); (**b**) microstructure of the granite, composed of quartz (Qtz), K-feldspar (Kfs), sericitized plagioclase, muscovite and biotite; (**c**) andesitic (And) exotic block (Jan Golonka during sampling for scale), in situ within the marly matrix; (**d**) photomicrograph showing the contact between dark (And-C) and light (And-J) parts of the andesitic block, with mudstone xenoliths (MDS); (**e**) insert showing the remnants of pyroxene (Px) and albitized plagioclase (Pl).

The study area is located within the Subsilesian Nappe. Originally occupying a structural position between the Silesian and the Skole nappes, the Subsilesian Nappe exposures south of Kraków are limited to small tectonic windows forming belts within the Silesian Nappe and along the northern boundary of the Magura Nappe (Figure 1c). The sampled area is located in a belt stretching over a distance of several kilometers along the boundary of the Magura Nappe and is known as the Żegocina Zone sensu Skoczylas–Ciszewska [16]. In the Żegocina Zone, a series of E–W trending structures are associated with the exposure of the Subsilesian nappe [9,16], and the zone is interpreted to represent a tectonic mélange. The Subsilesian Nappe is composed mainly of Upper Cretaceous and Lower Paleogene carbonate deposits, which were deposited in the Subsilesian Sedimentary Zone, an uplifted high that separates the Silesian and Skole basins [4,17,18]. The central part of this high is inferred to have been composed of crystalline basement rocks and

is termed the Subsilesian Ridge. This paleogeographic entity, which is now destroyed, supplied crystalline basement blocks to the slope and basinal areas. The crystalline blocks occur within marly slope deposits. These strongly tectonized Campanian–Maastrichtian grey marls contain different types of lithology, including limestones, gneisses, granitoids and andesites [19]. Two samples of c. 10 kg each were extracted from large rounded blocks of grey andesite (3 m in diameter) and a pale, fine-grained granitoid (4 m in diameter), in the Pluskawka Stream valley near the villages of Nowe Rybie and Kamionna in the Beskid Wyspowy Range (Figure 1c, N 49°47 15,8″, E 20°21 03,4″).

3. Analytical Techniques

3.1. Microscopy

Petrographic analyses of thin sections were undertaken at the Institute of Earth Sciences in the University of Silesia using an Olympus BX-51 microscope to constrain textural and microstructural relationships and to determine the presence of zircon.

3.2. Electron Probe Micro-Analyses (EPMA)

Microprobe analyses of the main rock-forming and accessory minerals were carried out at the Inter-Institutional Laboratory of Microanalyses of Minerals and Synthetic Substances, Warsaw, using a CAMECA SX-100 electron microprobe. The analytical conditions employed an accelerating voltage of 15 kV, a beam current of 20 nA, counting times of 4 s for peak and background and a beam diameter of 1–5 μm. Reference materials, analytical lines, diffracting crystals, mean detection limits (in wt%) and uncertainties were as follows: rutile—Ti (Kα, PET, 0.03, 0.05), diopside—Mg (Kα, TAP, 0.02, 0.11), Si—(Kα, TAP, 0.02, 0.21), Ca—(Kα, PET, 0.03, 0.16), orthoclase—Al (Kα, TAP, 0.02, 0.08), and K (Kα, PET, 0.03, 0.02), albite—Na (Kα, TAP, 0.01, 0.08), hematite—Fe (Kα, LIF, 0.09, 0.47), rhodonite—Mn (Kα, LIF, 0.03, 0.10), phlogophite—F (Kα, TAP, 0.04, 0.32), tugtupite—Cl (Kα, PET, 0.02, 0.04), Cr_2O_3—Cr (Kα, PET, 0.04, 0.01), ZirconED2—Zr (Lα, PET, 0.01, 0.01), Nb_2O_3-MAC—Nb (Lα, PET, 0.09, 0.01), V_2O_5—V (Kα, LIF, 0.02, 0.01), YPO_4—Y (Lα, TAP, 0.05, 0.05), CeP_5O_{14}—Ce (Lα, LPET, 0.09, 0.02), $NdGaO_3$—Nd (Lβ, LIF, 0.31, 0.24), ThO_2—Th (Mα, LPET, 0.09, 0.09), UO_2—U (Mα, LPET, 0.16, 0.13).

3.3. Whole-Rock Chemical and Isotope Analyses

Whole-rock analyses were undertaken by X-ray fluorescence (XRF) for major and large ion lithophile trace elements (LILE), and by fusion and ICP-MS for high field strength elements (HFSE) and rare earth elements (REE) at Bureau Veritas Minerals (Canada). Preparation involved lithium borate fusion and dilute digestions for XRF and lithium borate decomposition or aqua regia digestion for ICP-MS. LOI was determined at 1000 °C. Uncertainties for most of the major elements are 0.01%, except for SiO_2, which is 0.1%. REE were normalized to C1 chondrite [20].

The Sm-Nd analytical work was performed at the Laboratory of Geochronology, Department of Lithospheric Research, University of Vienna. Results are based on ion chromatography TIMS procedures. Sample digestion for Nd–Sr analysis was performed in Savillex® beakers using an ultrapure 4:1 mixture of HF and HNO_3 for 10 days at 110 °C on a hot plate. For whole rock powders, a minimum dissolution time of 3 weeks was applied to ensure maximum leaching of the REEs from refractory material such as zircon. After evaporating the acids, repeated treatment of the residue using HNO3 and 6.0 N HCl resulted in clear solutions for all samples. The REE fraction was extracted using AG®50W-X8 (200–400 mesh, Bio-Rad) resin and 4.0 N HCl. Nd was separated from the REE fraction using Teflon-coated HdEHP, and 0.22 N HCl as the elution media. Maximum total procedural blanks were 50 pg for Nd and were taken as negligible. Nd was run as metal on an Re double filament, using a ThermoFinnigan®Triton MC TIMS. A $^{143}Nd/^{144}Nd$ ratio of 0.511841 ± 0.000005 (n = 5) was determined for the La Jolla (Nd) international standard, during the period of investigation. Within-run mass fractionation for Nd isotope

compositions was corrected to $^{146}Nd/^{144}Nd = 0.7219$. Uncertainties on the Nd isotope ratio are quoted as 2 σm.

3.4. Mineral Separation and Imaging

Zircon crystals were separated using standard techniques (crushing, hydro-fracturing, washing, Wilfley shaking table, Frantz magnetic separator and hand picking). Mineral separation was carried out at the Institute of Geological Sciences at the Polish Academy of Sciences, Kraków, Poland. The crystals were cast in 25 mm diameter epoxy resin mounts, ground and polished to half-thickness to expose the grain interiors. Internal mineral textures were then characterized by back-scattered electron (BSE) and cathodoluminescence (CL) imaging, using a FET Philips 30 scanning electron microscope with a 15 kV accelerating voltage and a beam current of 1 nA at the Institute of Earth Sciences, University of Silesia, Sosnowiec, Poland.

3.5. LA-ICP-MS U-Pb Dating

LA-ICPMS U-Pb age zircon and apatite data were acquired using a Photon Machines Analyte Excite 193 nm ArF excimer laser-ablation system with a HelEx 2-volume ablation cell coupled to an Agilent 7900 ICPMS at the Department of Geology, Trinity College Dublin, Ireland. The instruments were tuned using NIST612 standard glass to yield Th/U ratios of unity and low oxide production rates (ThO+/Th+ typically <0.15%). A quantity of 0.4 l min^{-1} He carrier gas was fed into the laser cell, and the aerosol was subsequently mixed with 0.6 l min^{-1} Ar make-up gas and 11 mL min^{-1} N_2. For zircon, data reduction of the raw U-Pb isotope data was performed through the "VizualAge" data reduction scheme [21] in the freeware IOLITE package [22]. For apatite, the "VizualAge_UcomPbine" data reduction scheme [23], which can account for variable common Pb in the apatite standards, was employed. Sample-standard bracketing was applied after the correction of downhole fractionation to account for long-term drift in isotopic or elemental ratios by normalizing all ratios to those of the U-Pb reference standards. Final age calculations were made using the Isoplot add-in for Excel [24].

3.5.1. U-Pb Zircon Dating

For zircon dating, a repetition rate of 11 Hz and a circular spot of 24 µm were employed. Eleven isotopes (^{49}Ti, ^{91}Zr, ^{175}Lu, ^{202}Hg, ^{204}Pb, ^{206}Pb, ^{207}Pb, ^{208}Pb, ^{232}Th, ^{235}U and ^{238}U) were acquired during each analysis, which comprised 27 s of ablation and 12 s washout, the latter portions of which were used for the baseline measurement. In addition, 91500 zircon ($^{206}Pb/^{238}U$ TIMS age of 1065.4 ± 0.6 Ma; [25]) was used as the primary U-Pb calibration standard. The secondary standards GZ-7 zircon ($^{206}Pb/^{238}U$ TIMS age of 530.26 Ma ± 0.05 Ma; [26]), Plešovice zircon ($^{206}Pb/^{238}U$ TIMS age of 337.13 ± 0.37 Ma; [27]) and WRS 1348 zircon ($^{206}Pb/^{238}U$ TIMS age of 526.26 ± 0.70; [28]) yielded LA-ICPMS ages of 532.0 ± 2.2 Ma, 337 ± 1.6 Ma and 528.4 ± 3.2 Ma respectively.

3.5.2. U-Pb Apatite Dating

Apatite crystals were prepared as separates on polished epoxy mounts. A total of 29 isotopes (^{31}P, ^{35}Cl, ^{43}Ca, ^{51}V, ^{55}Mn, ^{88}Sr, ^{89}Y, ^{90}Zr, ^{139}La, ^{140}Ce, ^{141}Pr, ^{146}Nd, ^{147}Sm, ^{153}Eu, ^{157}Gd, ^{159}Tb, ^{163}Dy, ^{165}Ho, ^{166}Er, ^{169}Tm, ^{172}Yb, ^{175}Lu, ^{202}Hg, ^{204}Pb, ^{206}Pb, ^{207}Pb, ^{208}Pb, ^{232}Th and ^{238}U were acquired using a 60 µm laser spot, an 11 Hz laser repetition rate and a fluence of 2.5 J/cm^2. A ~1 cm sized crystal of Madagascar apatite that has yielded a weighted average ID-TIMS concordia age of 473.5 ± 0.7 Ma was used as the primary apatite reference material in this study. McClure Mountain syenite apatite (the rock from which the $^{40}Ar/^{39}Ar$ hornblende standard MMhb is derived) and Durango apatite were used as secondary standards. McClure Mountain syenite has moderate but reasonably consistent U and Th contents (~23 ppm and 71 ppm, [29]), and its thermal history, crystallization age (weighted mean $^{207}Pb/^{235}U$ age of 523.51 ± 2.09 Ma) and initial Pb isotopic composition ($^{206}Pb/^{204}Pb$ = 17.54 ± 0.24; $^{207}Pb/^{204}Pb$ = 15.47 ± 0.04) are

known from high-precision ID-TIMS analyses [30]. NIST 612 standard glass was used as the apatite trace-element reference material, and a crushed aliquot of Durango apatite that has been characterized by solution quadrupole-ICP-MS analyses [31], was used as the apatite trace-element secondary standard.

Common Pb in the apatite standards was corrected using a ^{207}Pb-based correction in VizualAge_UcomPbine and includes the propagation of the uncertainties in the age of the reference materials. Over the course of the analyses, McClure Mountain apatite (^{207}Pb/^{235}U TIMS age of 523.51 ± 2.09 Ma; [30]) and Durango apatite (31.44 ± 0.18 Ma; [32]) yielded weighted average 207Pb-corrected ages of 517.5 ± 3.5 Ma (MSWD = 2.3) and 31.82 ± 0.41 Ma (MSWD = 1.9), respectively. The McClure Mountain apatite age was anchored using a ^{207}Pb/^{206}Pb value of 0.88198 derived from an apatite ID-TIMS total U-Pb isochron [30]. All apatite REE contents were normalized to C1 chondrite [20].

4. Results

4.1. Petrography, Mineral Chemistry and Whole-Rock Chemistry of Exotic Blocks

4.1.1. Microgranite

Approximately 10 kg of microgranite (sample Pl-2) was extracted from a 4 m diameter block of fine-grained equigranular granitoid from Pluskawka Stream. Sample PL-2 is composed of quartz, zoned plagioclase (An_{24-12}), K-feldspar (Figure 2b), magmatic muscovite (Ti = 0.9–0.14 a.p.f.u; Table 1) and biotite (#mg = 0.19–0.21; Ti ~0.38 a.p.f.u.; Table 1), which is locally chloritized. Accessory minerals are ilmenite, REE-rich epidote (Table 2) and zircon. The equilibrium temperature of ternary feldspar is in the range of 392 °C to 455 °C (according to the Fuhrman and Lindsley model, [33] was (Table 3), assuming 200 MPa pressure.

Table 1. Representative microprobe analyses of biotite and muscovite with their crystal-chemical formulas recalculated for 22 O^{2-}.

Compound		**PL 2–Biotite (Bt)**				**PL 2–Muscovite (Ms)**			
	LoD	**Bt-1**	**Bt-2**	**Bt-3**	**Bt-4**	**Ms-1**	**Ms-2**	**Ms-3**	**Ms-4**
SiO_2 (wt.%)	0.04	34.45	34.24	34.72	33.67	46.29	46.90	46.40	46.56
TiO_2	0.06	3.26	3.17	3.26	3.22	1.35	1.28	0.91	0.97
Al_2O_3	0.03	18.09	18.16	18.44	18.09	33.06	33.88	35.38	35.30
Cr_2O_3	0.01	0.08	0.18	0.30	0.03	0.12	0.03	0.07	b.d.l
FeO	0.08	25.98	25.74	25.08	26.38	2.12	2.15	1.47	1.92
MgO	0.02	3.85	3.97	3.90	3.66	0.67	0.70	0.46	0.50
MnO	0.02	0.62	0.56	0.51	0.71	b.d.l.	0.07	0.06	b.d.l.
Na_2O	0.04	0.03	0.05	0.05	0.07	0.33	0.28	0.61	0.46
K_2O	0.05	9.28	9.56	9.26	9.39	10.55	10.28	10.30	10.58
Total		**95.64**	**95.63**	**95.52**	**95.22**	**94.49**	**95.50**	**95.66**	**96.29**
Si (apfu)		5.423	5.395	5.437	5.351	6.247	6.238	6.152	6.152
Al^{iv}		2.577	2.605	2.563	2.649	1.753	1.762	1.848	1.848
Al^{vi}		0.778	0.768	0.841	0.739	3.505	3.548	3.681	3.648
Ti		5.423	5.395	5.437	5.351	0.137	0.128	0.090	0.096
Cr		0.002	0.022	0.037	0.004	0.013	0.004	0.007	-
Fe		3.42	3.392	3.285	3.507	0.240	0.239	0.163	0.212
Mg		0.904	0.933	0.911	0.867	0.135	0.138	0.091	0.098
Mn		0.083	0.075	0.067	0.096	-	0.008	0.007	-
Na		0.009	0.016	0.015	0.022	0.086	0.073	0.157	0.119
K		1.863	1.921	1.85	1.904	1.817	1.745	1.742	1.783
#mg		0.20	0.21	0.21	0.19	0.36	0.36	0.35	0.32

#mg = Mg/(Fe + Mg + Mn); b.d.l.—below detection limit.

Table 2. Selected microchemical analyses and crystal chemical formulae of epidote and ilmenite from Pluskawka (Pl 2) microgranite.

		Epidote (Ep)			Ilmenite (Ilm)	
Compound	**LoD**	**Ep-1**	**Ep-2**	**Ep-3**	**Ilm-1**	**Ilm-2**
Nb_2O_5 (wt.%)	0.10	-	-	-	0.36	0.25
SiO_2	0.02	32.15	33.84	33.27	0.04	0.03
TiO_2	0.04	0.15	0.56	0.13	50.99	50.82
ThO_2	0.07	0.23	0.31	0.17	-	-
UO_2	0.01	b.d.l.	0.01	0.03	-	-
Al_2O_3	0.03	19.74	20.11	20.13	b.d.l.	b.d.l.
Fe_2O_3	0.10	11.76	10.91	11.19	11.69	10.67
V_2O_3	0.05	-	-	-	0.07	0.15
Y_2O_3	0.06	0.77	1.43	1.25	-	-
La_2O_3	0.04	4.46	2.99	3.25	-	-
Ce_2O_3	0.06	9.54	7.24	8.05	-	-
Pr_2O_3	0.28	0.77	0.99	0.73	-	-
Nd_2O_3	0.40	3.30	3.54	3.46	-	-
Sm_2O_3	0.20	0.55	0.85	0.46	-	-
Gd_2O_3	0.18	1.39	1.56	1.61	-	-
FeO	0.10	-	-	-	26.01	27.13
MnO	0.10	1.28	1.67	1.62	9.87	10.04
ZnO	0.02	-	-	-	0.06	0.10
MgO	0.02	0.08	0.08	0.06	-	-
CaO	0.04	11.49	10.91	11.77	-	-
Na_2O	0.03	0.04	0.15	0.04	-	-
H_2O_{calc}	-	1.65	1.69	1.65		
Total		**99.35**	**98.84**	**98.87**	**99.09**	**99.19**
		crystal-chemical formulea based on				
			25 O^{2-}		6 O^{2-}	
Nb (apfu)		-	-	-	0.009	0.006
Si		5.828	6.016	5.851	0.002	0.002
Ti		0.021	0.075	0.017	2.000	1.909
Th		0.010	0.013	0.007	-	-
U		0.000	0.000	0.001	-	-
Al		4.217	4.213	4.301	-	-
Fe^{3+}		1.604	1.459	1.527	0.311	0.289
V		-	-	-	0.002	0.006
Y		0.074	0.135	0.121	-	-
La		0.298	0.196	0.217	-	-
Ce		0.633	0.471	0.534	-	-
Pr		0.051	0.064	0.048	-	-
Nd		0.215	0.225	0.224	-	-
Sm		0.034	0.052	0.054	-	-
Gd		0.084	0.092	0.970	-	-
Fe^{2+}		-	-	-	1.246	1.252
Mn		0.197	0.251	0.248	0.436	0.442
Zn		-	-	-	0.002	0.004
Mg		0.021	0.020	0.017	-	-
Ca		2.233	2.077	2.287	-	-
Na		0.015	0.054	0.014	-	-
Σ_{REE}		1.315	1.100	2.047	-	-

This granitoid is weakly peraluminous (ASI = 1.065; Table 4), plotting on the high-K–calc-alkaline trend and within the volcanic arc granite field (Figure 3a,b).

Table 3. Modal composition and temperature estimate obtained using the Fuhrman and Lindsley [33] ternary feldspars geothermometry for feldspars from the exotic block from Pluskawka microgranite (Pl 2).

Feldspar Type/Composition	Ab	Or	An
K-feldspar and plagioclase			
plagioclase original/adjusted	0.822/0.808	0.008/0.010	0.163/0.182
alkali feldspar original/adjusted	0.031/0.100	0.904/0.899	0.004/0.001
Concordant temperature [°C]	412	412	412
Average temperature [°C]		412	
plagioclase original/odjusted	0.828/0.806	0.011/0.020	0.153/0.175
alkali feldspar original/adjusted	0.076/0.116	0.894/0.883	0.002/0.001
Concordant temperature [°C]	426	470	470
Average temperature [°C]		455	

Table 4. Chemical composition and selected petrological indices of the whole-rock samples of crystalline exotic blocks from the Pluskawka Stream.

		PLUSKAWKA		
Sample No.	**LoD**	**Pl 2**	**And-J**	**And-C**
SiO_2 (wt.%)	0.01	76.8	64.91	58.11
TiO_2	0.01	0.1	0.54	0.73
Al_2O_3	0.01	12.7	12.22	17.75
Fe_2O_{3T}	0.04	1.02	3.50	5.82
MnO	0.01	0.03	0.06	0.07
MgO	0.01	0.12	0.39	0.49
CaO	0.01	1.04	5.75	3.18
Na_2O	0.01	3.19	2.93	4.13
K_2O	0.01	4.49	3.45	5.38
P_2O_5	0.01	0.03	0.25	0.35
LOI	-	0.25	5.90	3.80
Total		99.77	99.90	99.81
Sr	0.5	72.5	218.00	275.60
Ba	1.0	593.00	714.00	1000.00
Rb	0.1	169.7	40.20	59.90
Th	0.2	17.10	12.00	16.60
U	0.1	5.10	3.50	2.60
Ga	0.5	13.40	12.30	17.00
Ni	0.1	1.10	20.00	32.00
Cr	5.0	-	62.00	90.00
Zr	0.1	96.00	138.10	196.30
Hf	0.1	3.30	3.30	4.90
Y	0.1	20.30	10.20	13.90
Nb	0.1	7.80	11.90	16.30
Ta	0.1	0.90	0.80	1.30
La	0.1	35.10	52.80	75.30
Ce	0.1	65.20	89.50	123.80
Pr	0.02	7.10	9.99	14.00
Nd	0.30	26.50	35.30	49.00

Table 4. *Cont.*

		PLUSKAWKA		
Sample No.	**LoD**	**Pl 2**	**And-J**	**And-C**
Sm	0.05	4.48	5.27	7.12
Eu	0.02	0.43	1.27	1.68
Gd	0.05	4.05	3.53	4.79
Tb	0.01	0.65	0.41	0.56
Dy	0.05	3.86	1.96	2.86
Ho	0.02	0.73	0.35	0.50
Er	0.03	2.06	0.96	1.42
Tm	0.01	0.3	0.13	0.18
Yb	0.05	2.27	0.92	1.17
Lu	0.01	0.32	0.14	0.19
ASI		1.07	0.66	1.01
Rb/Sr		2.34	0.18	0.22
#mg		0.32	0.31	0.25
Nd/Th		1.55	2.94	2.95
ΣREE		153.05	202.53	282.57
Eu/Eu*		0.31	0.90	0.88
Ce_N/Yb_N		7.54	25.55	27.79
T_{Zr} [°C]		758	N.A.	N.A.

#mg = Mg/(Fe + Mg + Mn).

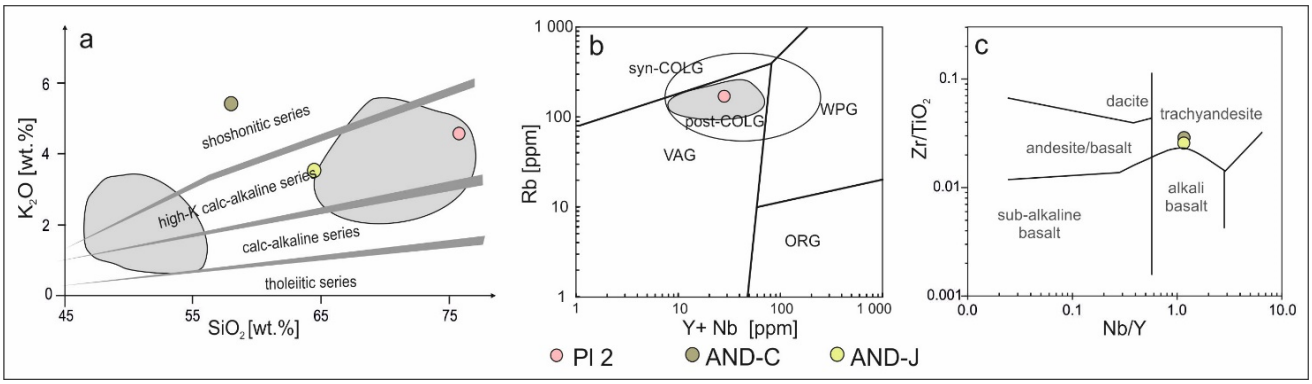

Figure 3. The Pluskawka microgranite and andesite plotted on: (**a**) K_2O versus SiO_2 classification diagram after using method presented in [34]; (**b**) discrimination diagram using method presented in [35]; (**c**) discrimination diagram using method presented in [36]. Gray areas are data from Mikulski et al. [37].

The granite yields a relatively low Zr saturation temperature (758 °C), high Rb/Sr ratio (2.34) and low Th/U ratio (3.35; Table 3). Chondrite (C1)-normalized REE patterns are characterized by a distinct negative Eu anomaly (Eu/Eu* = 0.31) and weak REE fractionation (Ce_N/Yb_N = 7.54; Table 4; Figure 4a). On a primitive mantle-normalized multi-element plot, enrichment in large ion lithophile elements (LILE) and negative Ti and P anomalies are noted (Figure 4b).

4.1.2. Andesite

Two samples (And-J and And-C), weighting approximately 10 kg each, were extracted from a 1.5 m in diameter block of andesite. Two different rock types were recognized in the samples—a light-grey variety with porphyritic texture and a dark-reddish, equigranular, fine-grained facies containing several small fragments of mudstone (1–3 cm in size). The mineral composition of both rock types is similar and consists of albitized plagioclase, chloritized biotite, spinel and sporadic remnants of pyroxene (Figure 2b) [38].

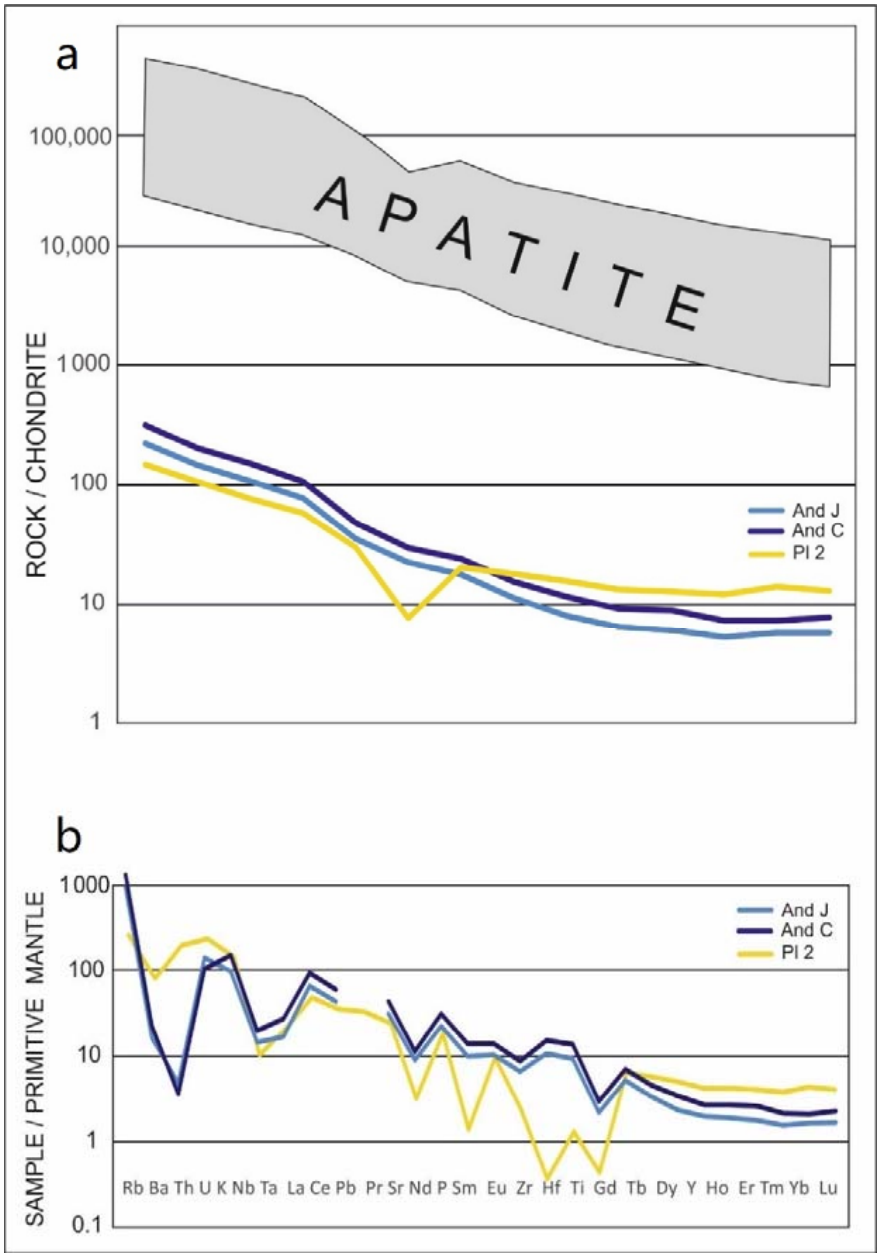

Figure 4. (**a**) Chondrite (C1)-normalized REE patterns of the microgranitoid (Pl 2) and andesite (And) from Pluskawka, with apatite from PL 2 (grey area); (**b**) primitive mantle normalized multi-element patterns of the analysed PL 2 and And exotic blocks from Pluskawka stream. Normalization values after McDonough and Sun [20].

On a Zr/TiO_2 vs Nb/Y diagram [35], both samples plot within the trachyandesite field (Figure 3c). On a multi-element plot, Nb and Ta negative anomalies are noted (Figure 4b). Chondrite (C1)-normalized REE patterns show moderate fractionation (Ce_N/Yb_N = 26.8–29.15) and very flat Eu anomalies (Eu/Eu* = 0.88–0.90; Table 4; Figure 4a). Due to the secondary alteration, the relatively mobile LILE were not used for geochemical discrimination purposes.

The cathodoluminescence images of zircons and apatites are shown in Figure 5.

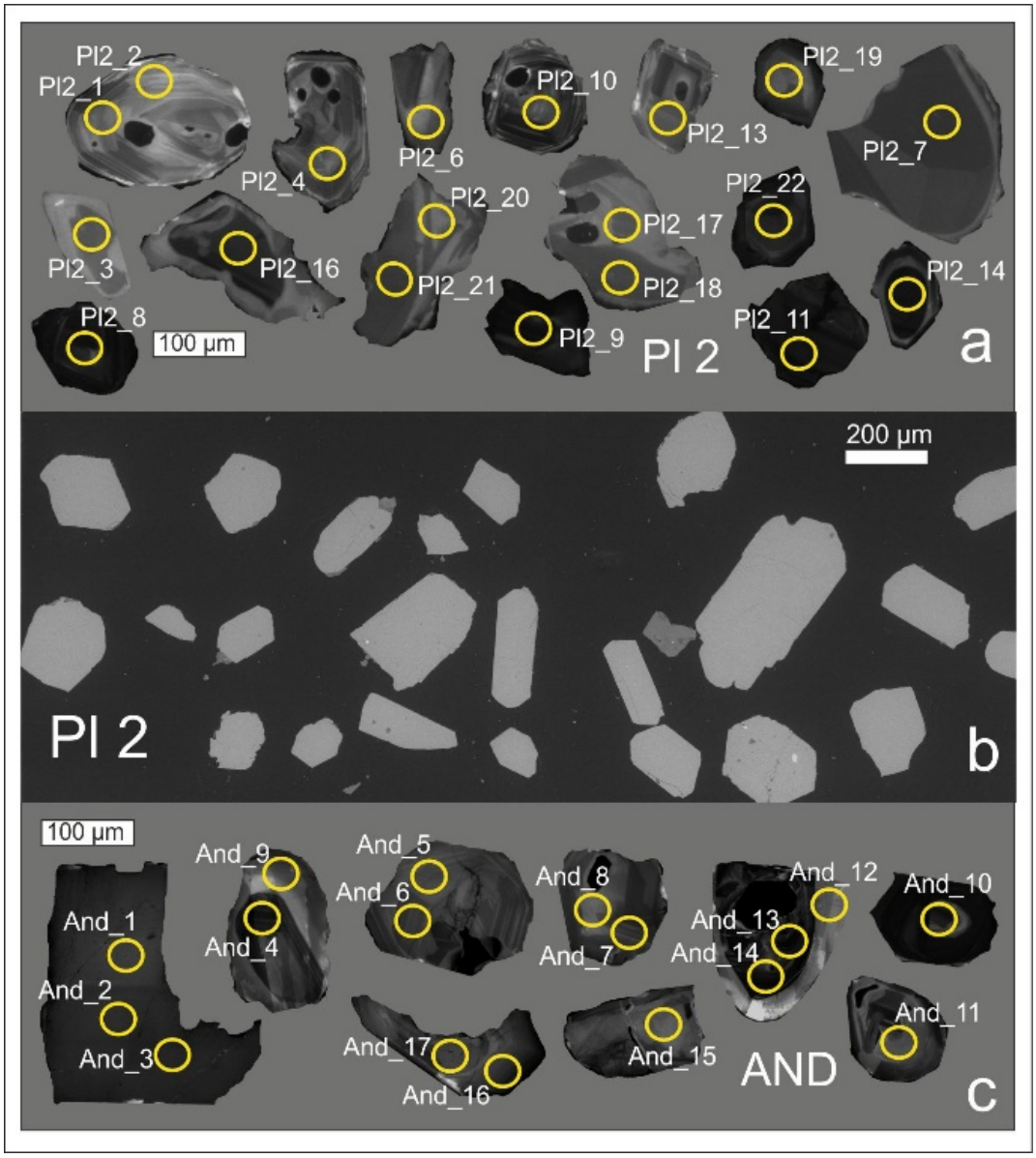

Figure 5. Cathodoluminescence (CL) images of zircon crystals from the microgranitoid (**a**)—Pl 2, apatite from microgranitoid (**b**)—PL 2 and andesite (**c**)—And from Pluskawka. Analytical spots and analyses numbers (see Table 5) are marked as circles.

Table 5. LA-MC-ICP-MS U–Pb zircon data from Pluskawka microgranite and andesite.

Sample No.	Pb^{207}/U^{235}	2σ	Pb^{206}/U^{238}	2σ	Rho	$^{207}Pb/^{235}U$ Age [Ma]	2σ	$^{206}Pb/^{238}U$ Age [Ma]	2σ	U [ppm]	Th [ppm]	Th/U
Microgranitoid												
Magmatic zircon crystals—Variscan												
PL2_1	0.335	0.026	0.0449	0.0019	0.024733	293	10	283.4	7.1	219	384	1.75
PL2_2	0.341	0.026	0.0472	0.0019	0.19609	297	10	297.4	6.3	202	262	1.42
PL2_4	0.323	0.028	0.046	0.0019	0.14079	282	14	289.7	6.5	124.2	213	1.71
PL2_6	0.338	0.034	0.0472	0.002	0.11162	301	19	297.3	7.3	69.1	84	1.22
PL2_10	0.343	0.03	0.0461	0.0019	0.096029	299	15	290.5	6.5	322	691	2.15
PL2_13	0.329	0.029	0.0468	0.0019	0.011323	290	15	294.6	6.5	151.2	374	2.47
PL2_19	0.367	0.035	0.0474	0.002	0.23971	318	19	298.7	6.7	176.3	260.9	1.48

Table 5. *Cont.*

Sample No.	Pb^{207}/U^{235}	2σ	Pb^{206}/U^{238}	2σ	Rho	$^{207}Pb/^{235}U$ Age [Ma]	2σ	$^{206}Pb/^{238}U$ Age [Ma]	2σ	U [ppm]	Th [ppm]	Th/U
Concordia age = 293.2 ± 4.1 Ma; MSWD = 0.31												
Inherited zircon crystals—Neoproterozoic												
PL2_3	0.94	0.068	0.1074	0.0042	0.1809	673	15	659	11	227	157	0.69
PL2_16	0.804	0.067	0.097	0.004	0.22032	597	24	596	13	64.8	40.4	0.62
PL2_18	0.854	0.071	0.0989	0.0047	0.25292	632	21	608	19	284.9	129.2	0.45
PL2_20 *	0.932	0.079	0.0953	0.0045	0.82171	673	27	587	18	301.2	302.6	1.00
PL2_22 *	0.903	0.068	0.0935	0.0042	0.47181	662	22	576	16	423	150.8	0.36
Inherited zircon crystals–Archean												
PL2_7	6.376	0.42	0.3646	0.013	0.51946	2028	10	2003	21	427	410	0.97
PL2_8	5.628	0.38	0.3339	0.013	0.67559	1921	13	1856	27	392	318	0.81
PL2_9	6.403	0.43	0.3641	0.014	0.59429	2031	12	2001	22	563	665	1.18
PL2_11 *	8.68	0.68	0.358	0.017	0.86632	2299	39	1973	54	117	157	1.34
PL2_14 *	5.93	0.44	0.2566	0.011	0.83782	1961	30	1471	33	229	39.6	0.17
PL2_17	12.36	0.83	0.491	0.019	0.63744	2634	14	2574	31	658	376	0.57
PL2_21	2.155	0.17	0.1932	0.011	0.64341	1165	28	1138	45	469	119.4	0.25
Andesite												
Rims—Variscan												
And_9	0.343	0.025	0.0493	0.0011	0.2744	310.2	6.9	299.4	21.8	111.2	200.7	1.81
And_12	0.373	0.021	0.049	0.0012	0.1797	308.4	7.6	321.9	18.1	73.8	114.8	1.56
Concordia age = 310 ± 4.9 Ma; MSWD = 0.22												
Inherited cores and crystals—Neoproterozoic												
And_15	0.751	0.043	0.0904	0.0025	0.1835	557.9	15.4	568.8	32.6	38.3	29.55	0.77
And_5	0.834	0.041	0.1003	0.002	0.1204	616.2	12.3	615.8	30.3	61.4	50.5	0.82
And_6	0.84	0.043	0.1018	0.0027	0.1315	624.9	16.6	619.1	31.7	113	52	0.46
And_7	0.833	0.045	0.0979	0.0022	0.1854	602.1	13.5	615.3	33.2	45.8	25.65	0.56
And_8	0.881	0.04	0.1036	0.0028	0.3205	635.5	17.2	641.5	29.1	60.7	42.6	0.70
And_16	0.812	0.034	0.1017	0.0021	0.2615	624.4	12.9	603.6	25.3	104.4	80	0.77
And_17	0.864	0.04	0.0988	0.0032	0.2590	607.4	19.7	632.3	29.3	73.6	76.5	1.04
Concordia age = 618.4 ± 8.3 Ma; MSWD = 0.18												
And_1	1.025	0.044	0.1171	0.0024	0.2701	713.9	14.6	716.4	30.8	71.4	107.6	1.51
And_2	1.033	0.038	0.1175	0.0024	0.2079	716.2	14.6	720.4	26.5	73.4	115.5	1.57
And_3	1.04	0.039	0.1176	0.0024	0.3231	716.7	14.6	723.9	27.1	74.3	115.8	1.56
Concordia age = 716.9 ± 7.3 Ma; MSWD = 0.66												
Inherited zircon crystals—Archean												
And_4	13.36	0.25	0.4982	0.009	0.4992	2606.1	47.1	2705.4	50.6	206.6	183.9	0.89
And_10	11.4	0.36	0.441	0.013	0.6003	2355.1	69.4	2556.4	80.7	61.4	83.4	1.36
And_11	5.626	0.084	0.2261	0.004	0.3906	1314.0	23.2	1920.1	28.7	1095	113	0.10
And_13	17.48	0.29	0.5863	0.0098	0.7073	2974.4	49.7	2961.6	49.1	775	485	0.63
And_14	16.46	0.56	0.564	0.019	0.6219	2883.1	97.1	2903.9	98.8	413	278	0.67

4.2. Zircon and Apatite Characteristics and U-Pb Dating

4.2.1. Microgranitoid

Zircon crystals from the fine-grained granite sample from Pluskawka Stream (Pl 2) are colorless, short-prismatic, with aspect ratios of 1:1 to 2:1. Cathodoluminescence imaging reveals the presence of magmatic oscillatory zoning, locally overgrowing inherited cores showing very weak luminescence. We undertook 22 spot analyses on 19 zircon grains (Figures 5a and 6a). Seven magmatically zoned grains yielded a concordia age of 293.2 ± 4.1 (MSWD = 0.31; Figure 6b,c). Five subconcordant Neoproterozoic $^{206}Pb/^{238}U$ ages ranging from 587 Ma to 659 Ma were detected in both inherited cores and single crystals; older

$^{206}Pb/^{238}U$ ages of 1138 Ma, 1471 Ma, 1856 Ma, 1973 Ma, 2001 Ma, 2003 Ma, 2574 Ma were also found in both inherited cores and single crystals (Table 5; Figure 6a).

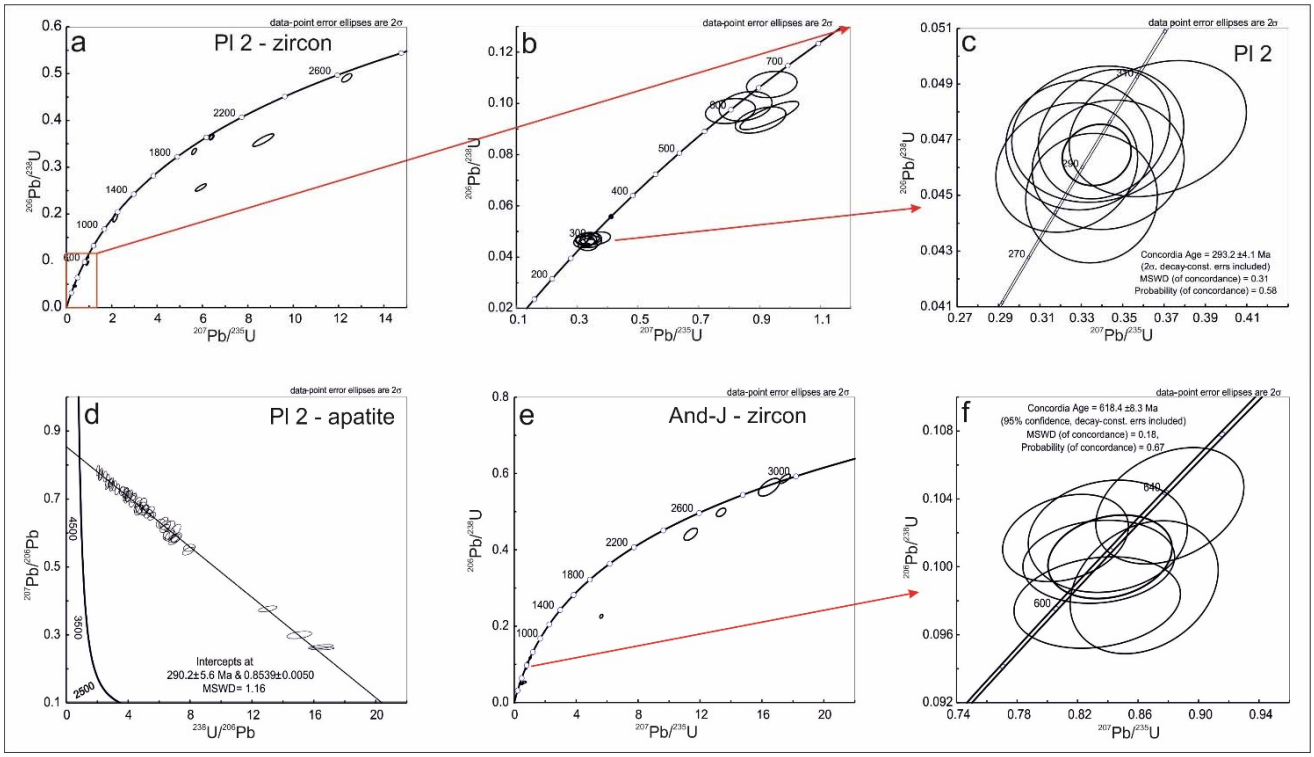

Figure 6. Concordia plots of LA-ICP-MS zircon and apatite analytical results: (**a**) microgranitoid from Pluskawka with inserts of Neoproterozoic zircon cores and Variscan zircons (**b**,**c**); (**d**) Tera–Wasserburg concordia plot for apatite from the Pluskawka microgranitoid; (**e**) concordia plot of the zircon crystals from the andesite, with an insert for Neoproterozoic inherited crystals age (**f**).

Apatite crystals are clear, translucent and idiomorphic hexagonal prisms, with aspect ratios ranging from 1.5:1 to 2.5:1 and long axes ranging from 100 to 250 µm (Figure 5b). We undertook 54 spot analyses on 42 apatite crystals. They are chemically zoned and rich in Mn (381–1317 ppm), Sr (656–3449 ppm), zoned with respect to REE, with $\sum_{REE}$ ranging from 3 192 ppm to 13 246 ppm (at rims and in cores, respectively) (Table S1). Their chondrite (C1)-normalized REE patterns show LREE enrichment (Ce/Yb = 12.7–99.9) and mostly negative Eu anomalies (Eu/Eu* = 0.21–0.87, with one exception at 1.43; Table S1; Figure 4a). Our 54 analyses from 42 grains yielded an unanchored Tera–Wasserburg lower intercept age of 290.2 ± 5.6 Ma with a $^{207}Pb/^{206}Pb$ initial ratio of 0.839 ± 0.0050 (MSWD = 1.16; Figure 6d; Table S2). The apatite grains plotted close to the intersection of the mafic I-type, alkaline and ultramafic fields on a Sr/Y vs $\sum_{LREE}$ biplot [39], with the majority of the grains plotting just inside the alkaline field.

4.2.2. Andesite

Nine zircon crystals from the andesite facies lacking visible mudstone clasts (And) were analyzed. The zircons are subhedral to anhedral, short-prismatic, with aspect ratios ranging from 1:1 to 2:1. We carried out 17 spot analyses (Table 5). Six analyses from magmatically zoned crystals (Figure 5c) showing moderate luminescence yielded a concordia age of 618.4 ± 8.3 Ma (Figure 6e,f). One zircon crystal with a homogeneous internal structure and weak luminescence yielded an age of 560.2 ± 13.7 Ma. One crystal exhibited homogeneous weak luminescence, typical of metamorphic zircon crystals; 3 analyses located within this grain yielded concordant age of 716.9 ± 7.3 Ma. Cathodoluminescence imaging reveals the presence of two inherited cores, mostly with weak luminescence, and

these yield concordant ages of 2958 and 2907 Ma, as well as discordant ages (Figure 6e, Tables S1 and S2). Two CL-bright, magmatically zoned rims which are 20 to 40 µm thick (Figure 5) yielded an age of 310 ± 4.9 Ma (Table 5).

5. Discussion

5.1. Petrogenetic Interpretation

The microgranite and andesite from Pluskawka share a volcanic arc affinity and positive Th and negative P and Ti anomalies on a primitive-mantle-normalized multi-element diagram (Figures 3b and 4b). These characteristics imply a crustal origin for the parent magma for both rock types. This is supported by the negative εNd^{293} value (−5.5, Table 6) and T_{DM} age of 1.45 Ga (Table 6) for the microgranite. This Nd isotope systematics are typical of granitoid rocks of the European Variscan belt and are interpreted to represent the Archean/Neoproterozoic basement that melted during Variscan orogenesis [40,41]. The mixed Paleoproterozoic /Neoproterozoic protolith is inferred from the U-Pb ages of inherited zircon crystals from the microgranite (PL 2) and andesite (AND), which both show Neoproterozoic and Paleoproterozoic (>2000 Ma) age ranges (Table 5). However, it may be unwise to assume that these samples represent Variscan magmatic rocks of volcanic arc affinity, as the geochemical characteristics could also have been inherited from the protolith ([42] and references therein). The very similar zircon and apatite ages (Figure 6) in microgranite sample Pl-2 (293.2 ± 4.1 Ma and 290.2 ± 5.6 Ma) imply very rapid cooling from crystallization temperatures to temperatures below the apatite closure temperature window (c. 450 °C) and thus support a hypabyssal origin.

5.2. Implications for Paleozoic Paleogeology

The analyzed rocks represent Late Carboniferous–Permian bimodal volcanic–plutonic activity (Figure 3a,b). The samples show lithological, geochemical and age similarities to the magmatic rocks from the Kraków–Lubliniec tectonic zone [36,41,43] as well as to the Carboniferous–Permian intraplate volcanic rocks that are widespread in the Romanian Moesia [43]. As the exotic blocks represent the basement that was eroded during the uplift of the Subsilesian Ridge, we assume that these magmatic rocks continued in the Protocarpathians to both the north-west and south-east (Figure 7).

The lineament connecting Tenczynek, Pluskawka and Moesia is related to the south-eastern extension of the Kraków–Lubliniec tectonic lineament as well as to the boundary between the Brunovistulia and Małopolska blocks [41–45]. According to Mazur et al. [46], this zone formed during the latest Carboniferous–Permian transtensional tectonic activity, contemporaneous with the Liplas–Tarnawa pull-apart basin located south of Kraków [47]. This lineament cuts across the Variscan structures within the Neoproterozoic basement of central Pangea (Figure 7). The Protocarpathian region is characterized by the Neoproterozoic basement overlain by Upper Paleozoic sedimentary sequences, similar to the Brunovistulia and Małopolska massifs [5,48,49]. As was previously mentioned, the other analyses of the Subsilesian exotics indicate the prevailing Neoproterozoic (Cadomian) age of the substratum in this area [5,13,14].

Table 6. Whole-rock Rb-Sr and Sm-Nd isotopic composition of the Pl 2 microgranite. T_{DM} calculated according to Liew and Hofmann [50] procedure.

Scheme 147.	Sm [ppm]	Nd [ppm]	$^{147}Sm/^{144}Nd$	$^{143}Nd/^{144}Nd$	±	$\varepsilon_{Nd}{}^{316}$	T_{DM}
Pl 2	4.48	26.5	0.102196	0.512175	0.000003	5.50	1.45

The Neoproterozoic rocks of the Protocarpathian basement were the source for the Variscan magmas formation, which subsequently was emplaced within this Late Variscan transpressional zone. The occurrence of the Late Paleozoic magmas is probably limited to this transpressional zone. The Neoproterozoic Outer Protocarpathian basement adjacent to the Laurussian margin was covered by the Paleozoic sedimentary rocks, including

Carboniferous coal-bearing strata (Figure 7) [50–55]. The Central Pangean Mountain Belt [54] was located west of the Outer Protocarpathian area (Figure 7). It included the Central Carpathian collisional zone

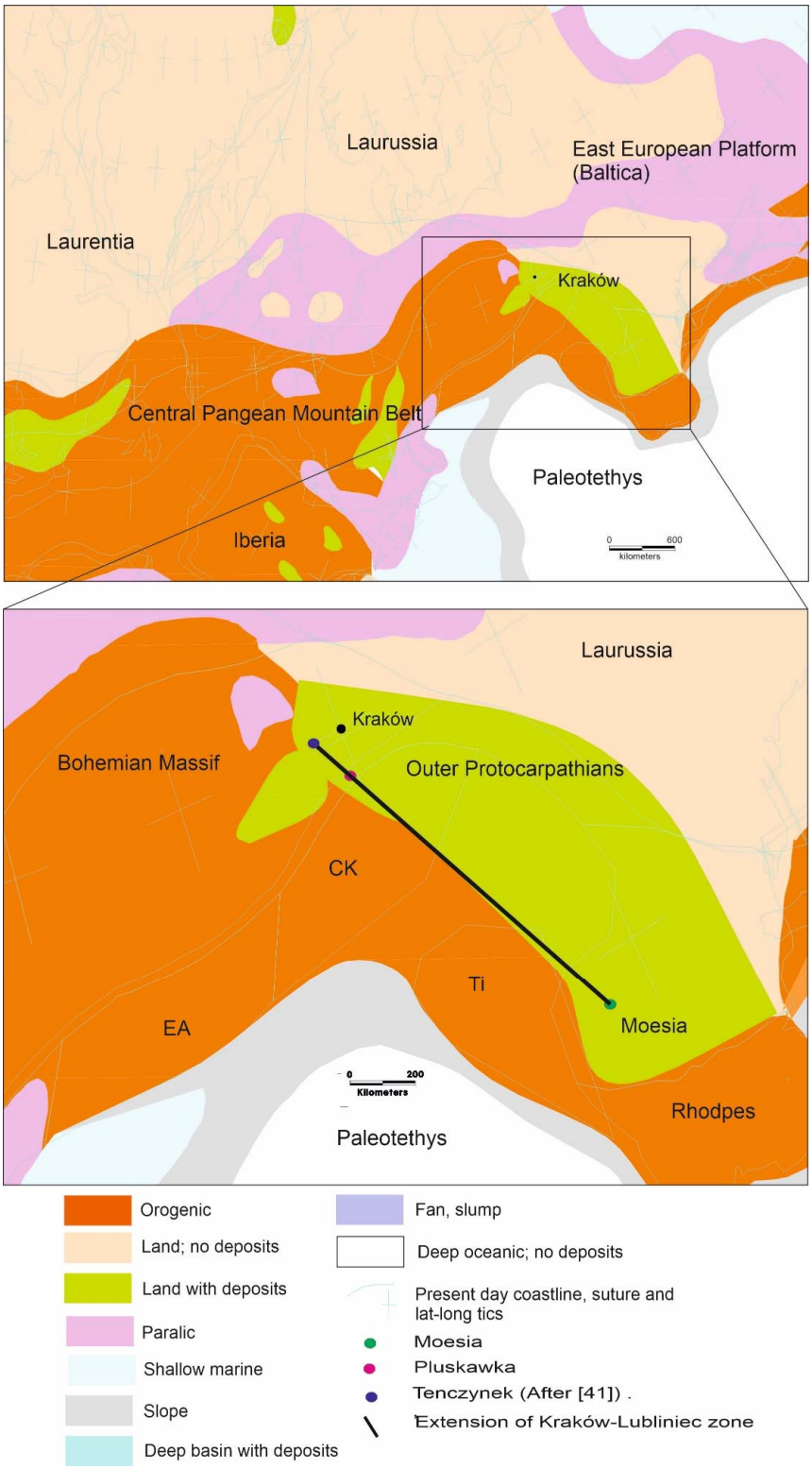

Figure 7. Paleogeography of the circum-Protocarpathian region during the latest Carboniferous–Permian. Abbreviations: CK = Central Carpathians; EA = Eastern Alps; Ti = Tisza.

5.3. Implications for Cretaceous–Paleogene Paleogeology

Epicontinental sedimentation continued in the Outer Protocarpathian region during Permian to Jurassic times [53]. The Protosilesian back-arc basin, containing syn-rift, post-rift and synorogenic deep-water sedimentary sequences was initiated during Late Jurassic times [3,18,54]. There is no evidence indicating the oceanic crust within this back-arc basin. The northward movement of the Central Carpathian plate, part of the larger ALCAPA (ALpine-CArpathian-PAnnonian) plate, caused progressive inversion and emergence of ridges during the Late Cretaceous. These ridges separated a series of newly formed basins [3,18,56]. The Subsilesian Ridge (Figure 8) separated the Silesian and Skole basins, which were later inverted to form the Silesian and Skole Nappes.

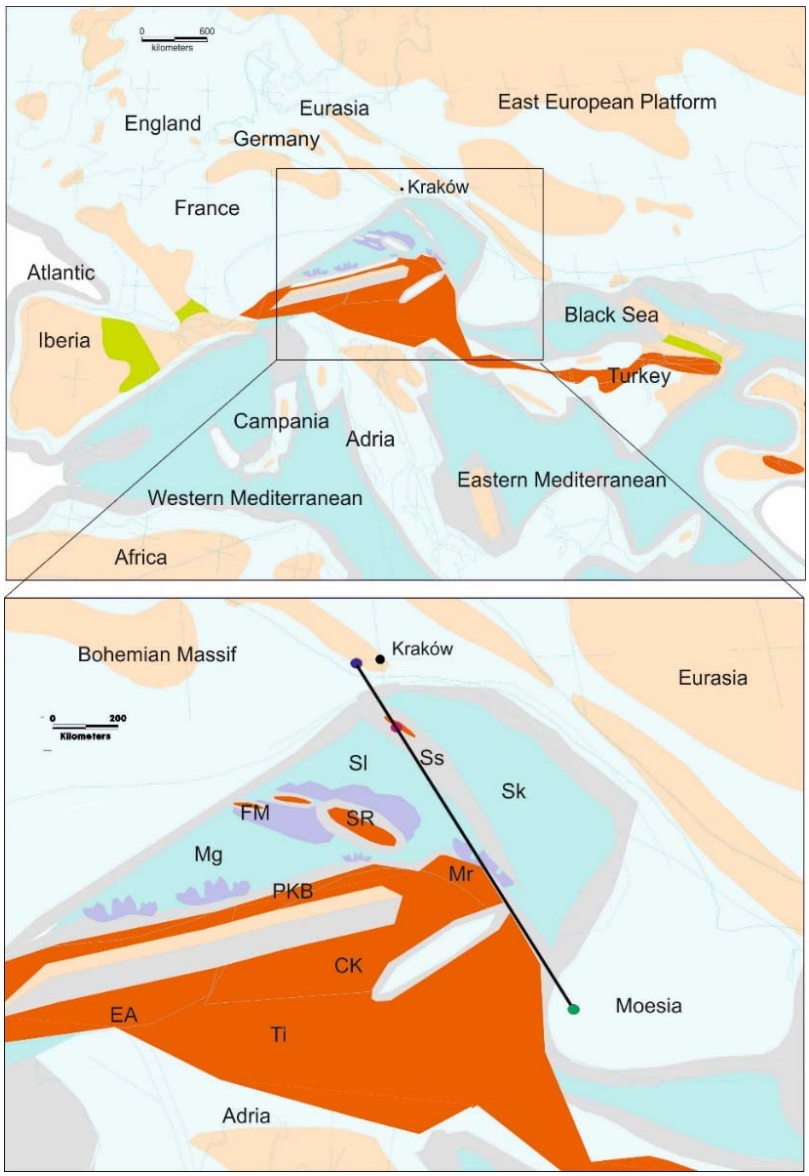

Figure 8. Paleogeography of the circum-Protocarpathian region during the Late Cretaceous–Paleocene. Legend as in Figure 7. Abbreviations: CK = Central Carpathians; EA = Eastern Alps; FM = Fore-Magura Basin; Mg = Magura Basin; Mr = Marmarosh Masssif; PKB = Pieniny Klippen Belt; Sk = Skole-Tarcău Basin; SR = Silesian Ridge; Ss = Subsilesian Ridge and sedimentary area; Ti = Tisza.

The Subsilesian Ridge, the source of the exotic clasts, was surrounded by a slope region characterized by mixed pelagic and turbiditic sedimentation that corresponds to the Subsilesian Sedimentary Zone. The large size of these blocks (more than 1 m in diameter, locally up to some tens of meters or even more than 100 m in diameter—see [14])—indicates short transport distances and intense tectonic activity during the deposition of the host Campanian–Maastrichtian grey marls [57] on the slope of the Subsilesian Ridge. This tectonic activity may have triggered earthquakes (see e.g., [58]) and produced mélange complexes.

This transpressional tectonic zone (Żegocina Zone) is regarded as a segment of the Kraków–Moesia fault zone in the basement and indicates rejuvenation of an older Paleozoic tectonic lineament. The position of the Żegocina Zone 100 km south of Kraków (see also [51]) and its link to the Kraków–Moesia lineament allow for a more precise palinspastic reconstruction of the Late Cretaceous–Paleocene Outer Carpathian basins (Figure 8). The suggested orientation of the Subsilesian Ridge (Figure 8) is consistent with the geometry of the Skole Basin that is quite narrow south of Kraków yet wide in eastern Poland, Ukraine and Romania [12,18,52,56]. According to Kováč et al. [59], two units related to the Subsilesian Nappe existed during Paleogene times: the Subsilesian Basin and the Subsilesian Ridge. The orientation of their ridge is similar to our paleogeography (Figure 8). According to Golonka et al. [18], the Subsilesian Ridge and slope constituted the Subsilesian Sedimentary Area. The Pluskawka exotics were deposited within the marly facies in the Subsilesian Sedimentary Area/Subsilesian Basin located next to the European Platform with Neoproterozoic basement. This area was situated around 100 km south of Kraków. It moved and now is about 30 km south of Kraków.

6. Conclusions

1. Exotic blocks of Late Carboniferous–Permian magmatic rocks are found in Campanian–Maastrichtian grey marls of the Subsilesian Nappe. This magmatic activity is also found outside the Carpathian Belt and can be linked to a Late Paleozoic transtensional zone, which is a continuation of the Lubliniec–Kraków Zone that extends under the Carpathians to Moesia.
2. This Late Paleozoic transtensional zone was probably reactivated during the Late Cretaceous under a transpressional regime within the Żegocina tectonic zone, which caused the uplift of the Subsilesian Ridge and intensive erosion.

Supplementary Materials: The following are available online at https://www.mdpi.com/article/10.3390/min11060571/s1, Table S1: Representative LA-ICP-MS U-Pb apatite data from the Pluskawka stream, Poland; Table S2: Trace elements content in apatite from Pluskawka microgranite (PL 2).

Author Contributions: J.G., corresponding author, project formulation, fieldwork and sampling, paleotectonic reconstructions, final discussions; A.G., corresponding author, project formulation, fieldwork, zircon selection, U-Pb age calculation and presentation, petrological description and interpretation, final discussion; A.W., fieldwork, sampling, lithological correlations, geological map preparation, final discussion; K.S., fieldwork, zircon imaging by cathodoluminescence, petrological descriptions, final discussion; D.C., U-Pb data reduction, U-Pb age calculations, final discussions and editing; F.D., U-Pb analysis. All authors have read and agreed to the published version of the manuscript.

Funding: This study was supported by National Science Centre (NCN) grant 2016/23/B/ST10/01896 given to J.G., A.G., A.W. and K.S., D.C. acknowledges past and present support from Science Foundation Ireland through research grants 12/IP/1663, 13/RC/2092 and 13/RC/2092_P2 (iCRAG Research Centre), and 15/IA/3024. iCRAG is funded under the SFI Research Centres Programme and is co-funded under the European Regional Development Fund.

Acknowledgments: The authors thank Beata Marciniak-Maliszewska for her help during microprobe analyses, while Monika Horschinegg is acknowledged for the help in the Nd isotope whole-rock work. We are grateful to the reviewers. Their remarks help to improve significantly the paper.

Conflicts of Interest: The authors declare no conflict of interest. The funders had no role in the design of the study, in the collection, analyses or interpretation of data, in the writing of the manuscript, or in the decision to publish the results.

References

1. Von Raumer, J.F.; Neubauer, F. History of Geological Investigations in the Pre-Triassic Basement of the Alps. In *Pre-Mesozoic Geology in the Alps*; Springer Science and Business Media LLC: Berlin, Germany, 1993; pp. 55–63. [CrossRef]
2. Von Raumer, J.F.; Bussy, F.; Schaltegger, U.; Schulz, B.; Stampfli, G.M. Pre-Mesozoic Alpine basements—Their place in the European Paleozoic framework. *GSA Bull.* **2013**, *125*, 89–108. [CrossRef]
3. Golonka, J.; Gawęda, A.; Waśkowska, A. Carpathians. In *Encyclopedia of Geology*, 2nd ed.; Alderon, D., Elias, S.A., Eds.; Elsevier BV: Amsterdam, The Netherlands, 2021; pp. 372–381. [CrossRef]
4. Golonka, J.; Ślączka, A.; Waśkowska, A.; Krobicki, M.; Cieszkowski, M. Budowa geologiczna zachodniej części polskich Karpat zewnętrznych. In *Głębokomorska Sedymentacja Fliszowa—Sedymentologiczne Aspekty Historii Basenów Karpackich*; Krobicki, M., Feldman-Olszewska, A., Eds.; V Polska konferencja Sedymentologiczna: Warsaw, Poland, 2013; pp. 11–62. (In Polish)
5. Gawęda, A.; Golonka, J.; Waśkowska, A.; Szopa, K.; Chew, D.; Starzec, K.; Wieczorek, A. Neoproterozoic crystalline exotic clasts in the Polish Outer Carpathian flysch: Remnants of the Proto-Carpathian continent? *Int. J. Earth Sci.* **2019**, *108*, 1409–1427. [CrossRef]
6. Książkiewicz, M. Bathymetry of the Carpathian flysch basin. *Acta Geol. Pol.* **1975**, *25*, 309–368.
7. Cieszkowski, M.; Golonka, J.; Ślączka, A.; Waśkowska, A. Role of the olistostromes and olistoliths in tectonostratigraphic evolution of the Silesian Basin in the Outer West Carpathians. *Tectonophysics* **2012**, *568*, 248–265. [CrossRef]
8. Żytko, K.; Zając, R.; Gucik, S.; Ryłko, W.; Oszczypko, N.; Garlicka, I.; Nemčok, J.; Eliáš, M.; Menčik, E.; Stránik, Z. Map of the tectonic elements of the Western Outer Carpathians and their foreland. In *Geological Atlas of the Western Outer Carpathians and their Foreland*; Poprawa, D., Nemčok, J., Eds.; Państwowy Instytut Geologiczny: Warsaw, Poland, 1989.
9. Wójcik, A.; Czerwiec, J.; Krawczyk, M. *Detailed Geological Map of Poland, 1:50,000 Scale, Limanowa Sheet*; Państwowy Instytut Geologiczny-Państwowy Instytut Badawczy: Warsaw, Poland, 2009.
10. Plašienka, D.; Grecula, P.; Putiš, M.; Hovorka, D.; Kováč, M. Evolution and structure of the Western Carpathians: An overview. In *Geological Evolution of the Western Carpathians*; Grecula, P., Hovorka., D., Putiš, M., Eds.; Mineralia Slovaca—Monograph: Bratislava, Slovakia, 1997; pp. 1–24.
11. Golonka, J.; Krobicki, M.; Matyszkiewicz, J.; Olszewska, B.; Ślączka, A.; Słomka, T. Geodynamics of ridges and development of carbonate platform within the Carpathian realm in Poland. *Slovak Geol. Mag.* **2005**, *11*, 5–16.
12. Ślączka, A.; Kruglow, S.; Golonka, J.; Oszczypko, N.; Popadyuk, I. The general geology of the Outer Carpathians, Poland, Slovakia, and Ukraine. In *The Carpathians and Their Foreland: Geology and Hydrocarbon Resources*; Golonka, J., Picha, F., Eds.; American Association of Petroleum Geologists: Tulsa, OK, USA, 2006; pp. 221–258.
13. Budzyń, B.; Dunkley, D.J.; Kusiak, M.A.; Poprawa, P.; Malata, T.; Skiba, M.; Paszkowski, M. SHRIMP U-Pb zircon chronology of the Polish Western Outer Carpathians source areas. *Ann. Soc. Geol. Pol.* **2011**, *81*, 161–171.
14. Burda, J.; Woskowicz-Ślęzak, B.; Klötzli, U.; Gawęda, A. Cadomian protolith ages of exotic mega blocks from Bugaj and Andrychów (Western outer Carpathians, Poland) and their palaeogeographic significance. *Geochronometria* **2019**, *46*, 25–36. [CrossRef]
15. Gawęda, A.; Golonka, J.; Chew, D.; Waśkowska, A.; Szopa, K. Central European Variscan Basement in the Outer Carpathians: A Case Study from the Magura Nappe, Outer Western Carpathians, Poland. *Minerals* **2021**, *11*, 256. [CrossRef]
16. Skoczylas-Ciszewska, K. Budowa geologiczna strefy żegocińskiej. *Acta Geol. Pol.* **1960**, *10*, 484–592.
17. Cieszkowski, M.; Golonka, J.; Waśkowska-Oliwa, A. Tectonics and tectonic evolutionary stages of the Subsilesian Realm, Outer Carpathians. In Proceedings of the 18th Congress of the Carpathian-Balkan Geological Association: Scientific Annals of the School of Geology, Belgrade, Serbia, 3–6 September 2006; Volume 100, pp. 72–74.
18. Golonka, J.; Waśkowska, A.; Ślączka, A. The Western Outer Carpathians: Origin and evolution. *Z. Dtsch. Ges. Geowiss. Ger. J. Geol.* **2019**, *170*, 229–254. [CrossRef]
19. Skoczylas-Ciszewska, K. O występowaniu tzw. andezytów w strefie żegocińskiej Karpat fliszowych. *Zesz. Nauk. Agh.* **1956**, *9*, 143–154. (In Polish)
20. McDonough, W.F.; Sun, S.-S. The composition of the Earth. *Chem. Geol.* **1995**, *120*, 223–253. [CrossRef]
21. Petrus, J.A.; Kamber, B.S. VizualAge: A Novel Approach to Laser Ablation ICP-MS U-Pb Geochronology Data Reduction. *Geostand. Geoanalytical Res.* **2012**, *36*, 247–270. [CrossRef]
22. Paton, C.; Hellstrom, J.; Paul, B.; Woodhead, J.; Hergt, J. Iolite: Freeware for the visualisation and processing of mass spectrometric data. *J. Anal. At. Spectrom.* **2011**, *26*, 2508–2518. [CrossRef]
23. Chew, D.M.; Petrus, J.A.; Kamber, B.S. U–Pb LA–ICPMS dating using accessory mineral standards with variable common Pb. *Chem. Geol.* **2014**, *363*, 185–199. [CrossRef]
24. Ludwig, K.R. *Isoplot/Ex, v. 4.75*; Berkeley Geochronology Center Special Publication: Berkeley, CA, USA, 2012; p. 5.
25. Wiedenbeck, M.; Hanchar, J.M.; Peck, W.H.; Sylvester, P.; Valley, J.; Whitehouse, M.; Kronz, A.; Morishita, Y.; Nasdala, L.; Fiebig, J.; et al. Further characterization of the 91500 zircon crystal. *Geostand. Geoanalytical Res.* **2004**, *28*, 9–39. [CrossRef]

26. Nasdala, L.; Corfu, F.; Schoene, B.; Tapster, S.R.; Wall, C.J.; Schmitz, M.D.; Ovtcharova, M.; Schaltegger, U.; Kennedy, A.K.; Kronz, A.; et al. GZ7 and GZ8—Two Zircon Reference Materials for SIMS U-Pb Geochronology. *Geostand. Geoanalytical Res.* **2018**, *42*, 431–457. [CrossRef]
27. Sláma, J.; Košler, J.; Condon, D.J.; Crowley, J.L.; Gerdes, A.; Hanchar, J.M.; Schaltegger, U. Plešovice zircon—A new natural reference material for U–Pb and Hf isotopic microanalysis. *Chem. Geol.* **2008**, *249*, 1–35. [CrossRef]
28. Pointon, M.A.; Cliff, R.A.; Chew, D.M. The provenance of Western Irish Namurian Basin sedimentary strata inferred using detrital zircon U-Pb LA-ICP-MS geochronology. *Geol. J.* **2011**, *47*, 77–98. [CrossRef]
29. Chew, D.M.; Donelick, R.A. Combined apatite fission track and U-Pb dating by LAICPMS and future trends in apatite provenance analysis. In *Quantitative Mineralogy and Microanalysis of Sediments and Sedimentary Rocks*; Sylvester, P., Ed.; Mineralogical Association of Canada: Québec, QC, Canada, 2012; pp. 219–248.
30. Schoene, B.; Bowring, S.A. U–Pb systematics of the McClure Mountain syenite: Thermochronological constraints on the age of the Ar-40/Ar-39 standard MMhb. *Contrib. Miner. Pet.* **2006**, *151*, 615–630. [CrossRef]
31. Chew, D.M.; Babechuk, M.G.; Cogne, N.; Mark, C.; O'Sullivan, G.J.; Henrichs, I.A.; Doepke, D.; McKenna, C.A. (LA,Q)-ICPMS trace-element analyses of Durango and McClure Mountain apatite and implications for making natural LA-ICPMS mineral standards. *Chem. Geol.* **2016**, *435*, 35–48. [CrossRef]
32. McDowell, F.W.; McIntosh, W.C.; Farley, K.A. A precise 40Ar–39Ar reference age for the Durango apatite (U–Th)/He and fission-track dating standard. *Chem. Geol.* **2005**, *214*, 249–263. [CrossRef]
33. Fuhrman, M.L.; Lindsley, D.H. Ternary feldspars modelling and thermometry. *Am. Min.* **1988**, *73*, 201–215.
34. Peccerillo, A.; Taylor, S.R. Geochemistry of Eocene calc-alkaline volcanic rocks from the Kastamonu area, Northern Turkey. *Contrib. Miner. Pet.* **1976**, *58*, 63–81. [CrossRef]
35. Pearce, J.A.; Harris, N.B.W.; Tindle, A.G. Trace element discrimination diagrams for the tectonic interpretation of granitic rocks. *J. Petrol.* **1984**, *25*, 956–983. [CrossRef]
36. Winchester, J.; Floyd, P. Geochemical discrimination of different magma series and their differentiation products using immobile elements. *Chem. Geol.* **1977**, *20*, 325–343. [CrossRef]
37. Mikulski, S.Z.; Williams, I.S.; Markowiak, M. Carboniferous–Permian magmatism and Mo–Cu (W) mineralization in the contact zone between the Małopolska and Upper Silesia Blocks (south Poland): An echo of the Baltica–Gondwana collision. *Int. J. Earth Sci.* **2019**, *108*, 1467–1492. [CrossRef]
38. Parys, A. Petrogeneza i Wiek U-Pb Egzotyku Andezytowego z Pluskawki, Płaszczowina Podśląska; Karpaty Zewnętrzne. Master's Thesis, University of Silesia in Katowice, Katowice, Poland, 2020.
39. O'Sullivan, G.; Chew, D.; Kenny, G.; Henrichs, I.; Mulligan, D. The trace element composition of apatite and its application to detrital provenance studies. *Earth Sci. Rev.* **2020**, *201*, 103044. [CrossRef]
40. Moyen, J.F.; Laurent, O.; Chelle-Michou, C.; Couzinié, S.; Vanderhaege, O.; Zeh, A.; Villaros, A.; Gardien, V. Collision vs. subduction-related magmatism: Two contrasting ways of granite formation and implications for crustal growth. *Lithos* **2017**, *277*, 154–177. [CrossRef]
41. Słaby, E.; Breitkreuz, C.; Żaba, J.; Domańska-Siuda, J.; Gaidzik, K.; Falenty, K.; Falenty, A. Magma generation in an alternating transtensional–transpressional regime, the Kraków–Lubliniec Fault Zone, Poland. *Lithos* **2010**, *119*, 251–268. [CrossRef]
42. Żaba, J. The structural evolution of Lower Palaeozoic succession in the Upper Silesia Block and Małopolska Block border zone, southern Poland. *Int. J. Earth Sci.* **1999**, *166*, 1–162.
43. Seghedi, A.; Vaida, M.; Iordan, M.; Verniers, J. Paleozoic evolution of the Romanian part of the Moesian Platform: An overview. *Geol. Belg.* **2005**, *8*, 99–120.
44. Buła, Z.; Jachowicz, M.; Żaba, J. Principal characteristic of the upper Silesian block and Malopolska Block border zone (southern Poland). *Geol. Mag.* **1999**, *134*, 669–677. [CrossRef]
45. Kalvoda, J. Upper Devonian–Lower Carboniferous foraminiferal paleobiogeography and Perigondwana terranes at the Baltica–Gondwana interface. *Geol. Carp.* **2001**, *52*, 205–215.
46. Mazur, S.; Aleksandrowski, P.; Gągała, Ł.; Krzywiec, P.; Żaba, J.; Gaidzik, K.; Sikora, R. Late Palaeozoic strike-slip tectonics versus oroclinal bending at the SW outskirts of Baltica: Case of the Variscan belt's eastern end in Poland. *Acta Diabetol.* **2020**, *109*, 1133–1160. [CrossRef]
47. Poprawa, P.; Jarosinski, M.; Pepel, A.; Kiersnowski, H.; Jawor, E. Tectonic evolution of the Liplas-Tarnawa area—Analysis of subsidence, mesostructures, seismic and gravimetric data. *Int. J. Earth Sci.* **2001**, *174*, 143–160.
48. Kalvoda, J.; Babek, O.; Fatka, O.; Leichmann, J.; Melichar, R.; Nehyba, S.; Spacek, P. Brunovistulian terrane (Bohemian Massif, Central Europe) from late Proterozoic to late Paleozoic: A review. *Int. J. Earth Sci.* **2007**, *97*, 497–518. [CrossRef]
49. Żelaźniewicz, A.; Buła, Z.; Fanning, M.; Seghedi, A.; Żaba, J. More evidence on Neoproterozoic terranes in Southern Poland and southeastern Romania. *Geol. Q.* **2009**, *53*, 93–124.
50. Liew, T.C.; Hofmann, A.W. Precambrian crustal components, plutonic associations, plate environment of the Hercynian Fold Belt of central Europe: Indications from a Nd and Sr isotopic study. *Contrib. Miner. Pet.* **1988**, *98*, 129–138. [CrossRef]
51. Burtan, J.; Golonka, J.; Tomas, A.; Zając, R. Nowe znaleziska paleozoicznych węglanowych skał egzotycznych we fliszu polskich Karpat zewnętrznych; New finds of Paleozoic carbonate exotics in the Flysch of the Polish Outer Carpathians. *Geol. Q.* **1983**, *27*, 307–327.
52. Kotlarczyk, J. Węgiel we fliszu karpackim-kilka spostrzeżeń sedymentologicznych. *Ann. Soc. Pol. Tow. Geol.* **1979**, *18*, 37–150.

53. Ebner, F.; Vozárová, A.; Haas, J.; Kovács, S.; Kräutner, H.-G.; Krstić, B.; Szederkényi, T.; Jamičić, D.; Balen, D.; Belak, M.; et al. Devonian—Carboniferous pre-flysch and flysch environments in the Circum Pannonian Region. *Geolo. Carp.* **2008**, *59*, 159–195.
54. Vozár, J.; Ebner, F.; Vozárová, A.; Haas, J.; Kovács, S.; Sudar, M.; Bielik, M.; Péró, C. *Variscan and Alpine terranes of the Circum-Pannonian Region*; Geological Institute: Bratislava, Slovakia, 2010.
55. Oszczypko, N.; Krzywiec, P.; Popadyuk, I.; Peryt, T. Carpathian foredeep basin (Poland and Ukraine): Its sedimentary, structural, and geodynamic evolution. In *The Carpathians and Their Foreland: Geology and Hydrocarbon Resources AAPG Memoir*; Golonka, J., Picha, F.J., Eds.; American Association of Petroleum Geologists: Tulsa, OK, USA, 2006; Volume 84, pp. 221–258. [CrossRef]
56. Golonka, J.; Gahagan, L.M.; Krobicki, M.; Marko, F.; Oszczypko, N.; Ślączka, A. Plate-tectonic evolution and paleogeography of the circum—Carpathian Region. In *The Carpathians and Their Foreland: Geology and Hydrocarbon Researces: AAPG Memoir 84*; Golonka, J., Picha, F., Eds.; American Association of Petroleum Geologists: Tulsa, OK, USA, 2006; pp. 11–46.
57. Bielawska, J. Paleoecological Remarks about the Late Cretaceous Foraminiferids from the Frydek-Type Marls (Subsilesian Unit, Polish Outer Carpathians). Geologica Carpathica. Available online: http://www.geologicacarpathica.com/data/files/files/special%20issue/B/Bielawska.pdf (accessed on 16 April 2021).
58. Moscardelli, L.; Wood, L. Morphometry of mass-transport deposits as a predictive tool. *GSA Bull.* **2016**, *128*, B31221.1. [CrossRef]
59. Kováč, M.; Plašienka, D.; Soták, J.; Vojtko, R.; Oszczypko, N.; Less, G.; Ćosović, V.; Fügenschuh, B.; Králiková, S. Paleogene palaeogeography and basin evolution of the Western Carpathians, Northern Pannonian domain and adjoined areas. *Glob. Planet. Chang.* **2016**, *140*, 9–27. [CrossRef]